

***Ab initio* simulations of amorphous carbon nitrides**A. R. Merchant,^{1-3,*} D. R. McKenzie,^{1,2} and D. G. McCulloch³¹*Australian Key Centre for Microscopy and Microanalysis, University of Sydney, F09 NSW 2006, Australia*²*School of Physics, University of Sydney, A28 NSW 2006, Australia*³*Department of Applied Physics, RMIT University, GPO BOX 2476V Melbourne, 3001 Australia*

(Received 23 April 2001; revised manuscript received 3 July 2001; published 19 December 2001)

Density-functional *ab initio* molecular dynamics is used to study the incorporation of nitrogen into carbon networks. The resulting networks were analyzed using a Wannier-function technique for producing a localized orbital picture that provided us with a means of identifying bonding types of the nitrogen and carbon atoms within the disordered structures. Addition of nitrogen was found to cause a decrease in the fraction of sp^3 -bonded carbon and this effect is most severe at high density. These changes to carbon bonding are not confined to carbon atoms in the immediate vicinity of a nitrogen atom. The structure, and elastic and electronic properties of the networks are examined and compared with existing simulations and experimental observations. We found that removing electrons from the networks caused structural changes that could explain the two-state conductivity in amorphous carbon nitride memory devices.

DOI: 10.1103/PhysRevB.65.024208

PACS number(s): 61.43.Dq, 71.15.Pd

I. INTRODUCTION

Amorphous carbon (*a*-C) films have a variety of structural forms with a range of properties, for a review see McKenzie.¹ Interest in *a*-C has been stimulated by its many applications, and there has been considerable research exploring both its structure and properties using experimental and theoretical approaches. The addition of nitrogen to *a*-C to form an amorphous carbon-nitrogen alloy (*a*-C:N) is also of interest since certain useful properties result. In particular, nitrogen incorporation into carbon networks has been found to modify their electrical conductivity,² tribological characteristics,³ and chemical reactivity.⁴

At concentrations of less than 1%, nitrogen increases the conductivity² and modifies the Fermi energy in a manner analogous to the conventional *n*-type doping of silicon.⁵ At higher concentrations ($\approx 5\%$), the nitrogen induces a new Poole-Frenkel conductance mode in addition to the hopping mode also present at lower concentrations.⁶ The resulting two-state conductivity is of interest as a nonvolatile memory.

At higher nitrogen concentrations (5%–50%), the character of the material is observed to change, as the material develops a more layered structure, with sp^2 -bonded carbon the predominant form of carbon bonding. Another facet to the carbon-nitrogen system at high nitrogen concentration arises from the predictions of Liu and Cohen⁷ that a crystalline form of C_3N_4 , with structure analogous to β - Si_3N_4 , would have an extremely high bulk modulus.

Electron energy-loss near-edge structure (ELNES) studies² reveal the local density of unoccupied states at nitrogen or carbon atom sites and therefore can be used to determine the bonding configuration of the atom. At low nitrogen concentrations, in dense networks of tetrahedral amorphous carbon (*ta*-C), the nitrogen *K*-edge ELNES is similar to the carbon *K*-edge ELNES, which shows no $1s$ - π^* feature characteristic of sp^2 bonding. This has been taken as evidence that nitrogen dopes *ta*-C substitutionally at low concentrations. However, substitutional doping is not consistent with our previous studies⁸ in which a single nitrogen

atom is substituted for a carbon atom in a *ta*-C network and then relaxed. When nitrogen was substituted for an sp^2 -bonded carbon atom, the site remained as threefold coordinated, and a lone-pair orbital was developed. When nitrogen was substituted for a sp^3 -carbon atom, a bond was broken and the coordination of the site was reduced to three. The fourth bond was lengthened to accommodate the lone-pair orbital on the nitrogen atom. This latter effect shows that substitutional doping is not occurring in the conventional sense, where the bonding environment of the dopant atom is identical to the original host atom.

Amorphous carbon-nitrogen alloys can be synthesized using a number of energetic condensation methods, in which energetic carbon and nitrogen ions are combined to form a thin film. The experimental synthesis of a crystalline material with the formula C_3N_4 has proved most elusive, with most attempts resulting in an *a*-C:N alloy with a range of nitrogen concentrations.⁹

In this paper we reexamine the issue of nitrogen incorporation in *a*-C using *ab initio* molecular-dynamics methods to simulate the growth of the network by the “liquid-quench” method. In recent work, Marks, McCulloch, and McKenzie¹⁰ have shown that an amorphous structure prepared in a molecular-dynamics simulation by the liquid-quench method is essentially the same as one grown by atom-by-atom condensation. We believe the liquid-quench technique gives a more faithful representation of the experimental synthesis of *a*-C:N films than does the relaxation method of our previous work, because it allows a more complete exploration of the local environment surrounding the N atom.

In the analysis of our simulated networks we have used the Wannier-function technique for producing a localized orbital picture within a periodic supercell. This technique has been used by Silvestrelli *et al.*¹¹ in amorphous silicon. The number of Wannier-function centers between atoms identifies the bond type (double, single, or triple). In addition, Wannier functions enable us to identify lone pairs of electrons and types of carbon and nitrogen defects within our networks.

TABLE I. Bonding details for carbon and nitrogen atoms in all simulations. Higher nitrogen content promotes the formation of charged carbon defects at higher density.

Simulation (g/cm ³)	I C ₄ ⁰	II C ₃ ⁰	III C ₃ ⁺	IV C ₃ ⁻	V C ₂ ⁰	I N ₄ ⁺	II N ₃ ⁰	III N ₃ ⁺	IV N ₂ ⁰	V N ₂ ⁺
C ₆₂ N ₂ -2.45	14	40	3	4	1		1			1
C ₅₆ N ₈ -2.45	12	40	1	2	1		3	1	4	
C ₆₂ N ₂ -2.95	38	24					2			
C ₅₆ N ₈ -2.95	26	23	2	4	1	1	5	1	1	
C ₆₂ N ₂ -3.20	60	2					2			
C ₅₆ N ₈ -3.20	41	10	2	3			6	1	1	
Total	191	139	8	13	3	1	19	3	6	1

II. SIMULATION DETAILS

We employ the density-functional approach of Car and Parrinello, which uses a plane-wave expansion of the electronic wave functions. For this work the CPMD (Car-Parrinello molecular-dynamics) program developed and maintained by the Max Planck Institut für Festkörperforschung, Stuttgart, Germany, was used.¹² This program has been used previously to model carbon networks at various densities^{13–15} and AIBN networks.¹⁶ CPMD has also been used previously to study nitrogen defects in diamondlike amorphous carbon by Stumm, Drabold, and Fedders.¹⁷

Periodic boundary conditions and gamma point sampling of the Brillouin zone were used. Troullier Martins¹⁸ pseudopotentials in the Kleinmann-Bylander form were used to represent the carbon and nitrogen ion cores, with a Becke-Lee-Yang-Parr^{19,20} exchange and correlation functional.

The pseudopotential was checked against several aromatic carbon-nitrogen molecules (pyrazine, cyanogen, pyrrole, and imidazole). At the selected plane-wave cutoff of 50 Ry the computed bond lengths fell within 2% of reported values in all cases.

In this study the effect of density and nitrogen concentration was studied using seven different simulations of 64 atom networks using the “liquid-quench” methodology. Six simulations were at densities of 2.45, 2.95, and 3.2 g/cm³ with two nitrogen concentrations (corresponding to two and eight nitrogen atoms in 64, total) as summarized in Table I. A seventh simulation of 64 atoms was at a density of 2.7 g/cm³ and contained four nitrogen atoms; the choice of these parameters was made for comparison with an experimental carbon nitride study of Walters *et al.*²¹

The networks shown in Table I were formed using the local-density approximation (LDA) to density-functional theory (DFT). In the LDA, all orbitals are assumed to be doubly occupied, so no unpaired spin defects can be studied. This is a reasonable approximation to employ since it has been found that there is a low number of unpaired spins in amorphous carbon nitride.²² Also previous *ab initio* simulations of amorphous carbon^{13,14} have shown that the LDA is sufficient to describe bonding in *a*-C. Additional calculations were also performed using the local spin-density (LSD) approximation to DFT, which does not assume each orbital is

doubly occupied. LSD was used in order to check whether the LDA was inhibiting certain bonding configurations. The LSD approximation was also employed to study the effect of charge removal on the network structures.

In the “liquid-quench” method a randomized cubic lattice of atoms was allowed to melt, forming a liquid with a temperature above 4000 K that was allowed to equilibrate. The liquid was annealed at this temperature for 0.5 ps. The liquid was then quenched to 300 K following a Newtonian cooling equation of the form $T = 4000e^{-(ct)}$, where t is simulation time, and c is a constant determined by initial and final temperatures and quench time. The quenching time of 0.5 ps is comparable to the quench time expected for a thermal spike following the impact during deposition from an ion beam of energy 50 eV.²³ All structures were annealed at 300 K for an additional 0.5 ps to enable averaged structure statistics to be collected.

A method of generating maximally localized Wannier functions from the occupied Bloch states has been developed and implemented in the CPMD code.¹² In the Wannier-function analysis a unitary transform is applied to express the Bloch states as a sum of orthogonal, localized functions. However, even for the case of a single k -point calculation (used in this study), the unitary transform is not uniquely defined since each Kohn-Sham orbital can be multiplied by an arbitrary phase factor. Marzari and Vanderbilt²⁴ resolved this by requiring the total spread of Wannier functions to be minimized in real space. To simplify the analysis, rather than visualize the spatial structure of maximally localized Wannier functions, only the Wannier-function centers (WFC’s) are calculated. The location of the Wannier-function x coordinate x_n (and similarly, y_n and z_n) of the n th WFC is given by

$$x_n = -\frac{L}{2\pi} \text{Im} \ln \langle w_n | e^{-i(2\pi/L)x} | w_n \rangle, \quad (1)$$

where L is the length of the supercell and w_n is the n th maximally localized Wannier function. The full details of the calculation can be found elsewhere.^{11,25} The spread in real space of a single Wannier function can also be calculated and provides a measure of localization in real space. Defect states are expected to be less localized than bonding states.

The energies of the unoccupied states (Kohn-Sham orbitals) were calculated in order to derive the electronic density of states (EDOS) for the simulated structures. The Debye formula²⁶ for neutron diffraction was used to calculate the diffracted intensity $S(Q)$,

$$S(Q) = \sum_j \sum_j \frac{f_i f_j \sin(Q \cdot r)}{Q \cdot r}, \quad (2)$$

where $Q = 4\pi \sin(\theta)/\lambda$, r is the distance between atoms, f_i and f_j are the neutron-scattering lengths, and the sum is over all atoms. For WFC analysis the standard pair-correlation function $g(r)$ was calculated by treating the WFC as a third atomic species. For comparison to experiment the reduced radial distribution function²⁷ $G(r)$ was calculated using neutron-scattering lengths and the weighted combination of pair correlation functions. The distribution of ring sizes for

each network was calculated using the shortest path criteria described by Franzblau.²⁸

III. RESULTS AND DISCUSSION

A. Structural analysis using Wannier-function centers (WFC's)

Carbon and nitrogen atoms in our amorphous networks form single, double, or triple bonds with typical bonding arrangements shown in Figs. 1 and 2. Also shown is the location of WFC's using small black spheres. For a single (or σ) bond, one WFC is formed between two ions. Between two carbon ions, the WFC is found at the midpoint of the two ions with a spread in real space of ≈ 1.4 Å. This arrangement can be seen in Fig. 1(a) for an sp^3 -bonded C atom with four σ bonds. In a carbon-nitrogen bond, however, the WFC lies closer to the nitrogen ion, an indication of the ionicity of the bond, see Fig. 2(a). A double bond (or $\sigma + \pi$) forms two WFC's, at 0.7 Å from each other midway between the two ions with a spread of 1.5–1.7 Å. An example of this is Fig. 2(b). A triple bond ($\sigma + 2\pi$) forms three WFC's in a triangle between two ions, like in Fig. 2(d), where there is a triple bond-between an sp -bonded C and an sp -bonded N. The distance between each of the three WFC's is 0.5 Å, so the WFC's lie closer together in a triple bond than in a double bond.

Another common location of WFC's corresponds to electron lone pairs forming on nitrogen ions with a spread in real space of ≈ 1.8 Å, see Fig. 2(a). Where a lone pair has formed, a single WFC is found close (0.3–0.4 Å) to a nitrogen ion. All of the valence electrons in the networks form one of these three bond types (single, double, or triple) or lone pairs. Using these definitions of bonds/lone pairs within the simulated networks, the structures could be analyzed in detail. The number of WFC's around an ion enabled us to determine if the atom was sp , sp^2 , or sp^3 hybridized without the need to assume bond cutoff distances or coordination shells. In addition, we could identify the presence of defects or doping sites within our networks, which contained WFC's with a spread of >2 Å.

In addition to uncharged sp^3 (C_4^0), sp^2 (C_3^0), and sp (C_2^0) carbon sites, C_3^+ and C_3^- defect sites were observed, see Fig. 1(e). In the case of nitrogen, N_3^0 and N_2^0 neutral sites as well as N_4^+ , N_3^+ , and N_2^+ doping sites were observed in the networks. Table I shows the number of each of these bonding classifications for each of the networks studied. The most common nitrogen site was the uncharged N_3^0 site, where a nitrogen formed three single σ bonds to carbon atoms and a lone pair of electrons [see Fig. 2(a), for example]; the second most common nitrogen site was the uncharged N_2^0 site with an example shown in Fig. 2(c).

There were three ways nitrogen atoms formed charged defects. The first is shown in Fig. 2(b), which is an sp^3 hybridized nitrogen ion with four bonds. Because this nitrogen has only four valence electrons, it is an sp^3 hybridized N_4^+ defect site. The second way a nitrogen can bond and form a defect is when three σ and one π bond form, making it an N_3^+ site [see Fig. 2(e)]. As discussed earlier, the third

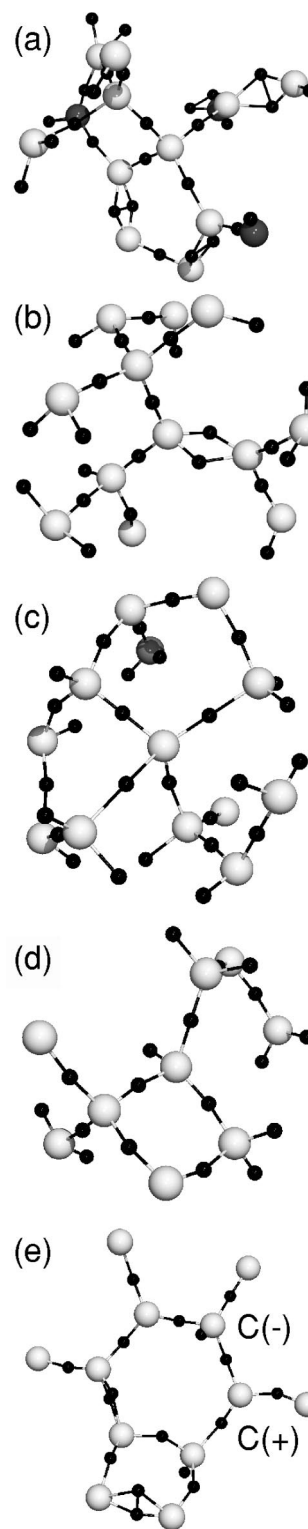


FIG. 1. Typical arrangements of WFC's (shown as small black spheres) around carbon ions forming single, double, and triple bonds. Some locations of the WFC also correspond to charged defects. Carbon atoms are shown as light gray, nitrogen atoms as dark gray.

way a nitrogen can form a defect is an sp nitrogen forming a triple bond with a carbon [see Fig. 2(d)]—this is termed an N_2^+ defect. We found no circumstances where the nitrogen atoms formed a negatively charged defect.

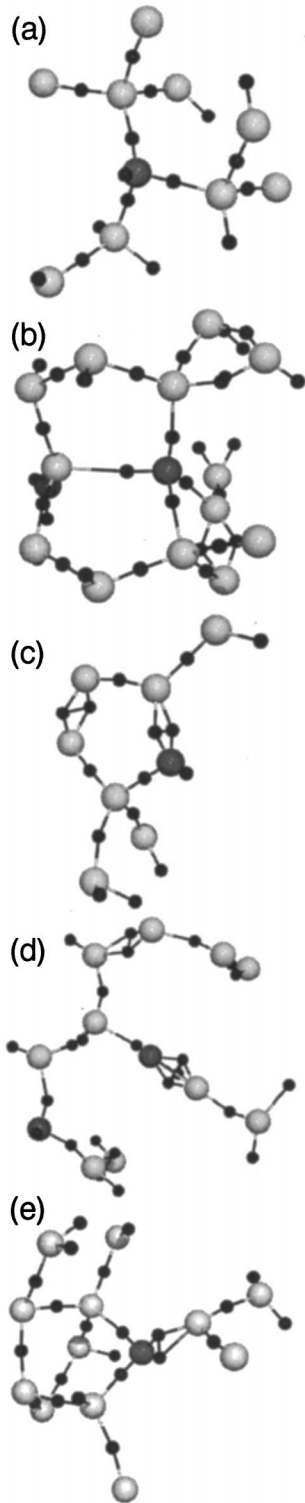


FIG. 2. Typical arrangements of WFC's (shown as small black spheres) around nitrogen ions forming single, double, and triple bonds. Some locations of the WFC also correspond to charged defects. Carbon atoms are shown as light gray, nitrogen atoms as dark gray.

B. Analysis of WFC-nitrogen-carbon partial $g(r)$'s

The ionic structure of the carbon-nitrogen networks was analyzed by visualizing the WFC's as a third species of

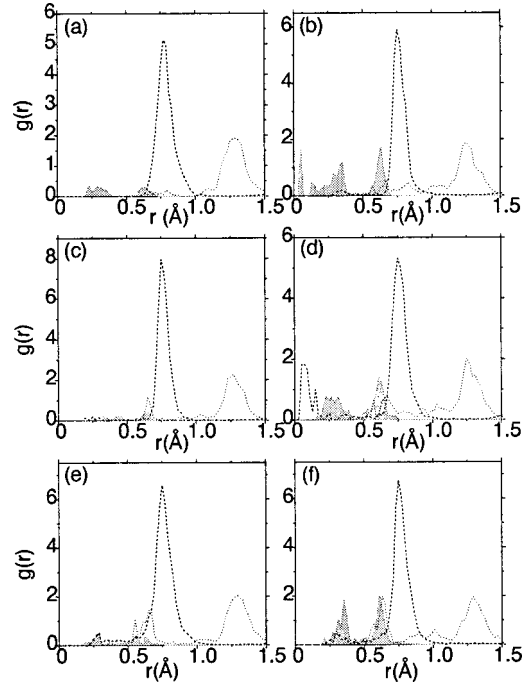


FIG. 3. The partial correlation functions C-WFC (dashed), N-WFC (shaded), and WFC. WFC (dotted) for the six simulations. From left to right is two (a), (c), and (e) and eight (b), (d), and (f) nitrogen, and from top to bottom is 3.2 (a) and (b), 2.95 (c) and (d), and 2.45 g/cm^3 (e) and (f). The distribution of distances indicates that there are a number of defect states.

atom. We monitored the evolution of the WFC's during a 300-K anneal, and then calculated the $g(r)$ correlation functions for the network. We found that in the C-N-WFC system the total $g(r)$ is too complicated, and we therefore show only partial $g(r)$ functions $g_{\text{C-WFC}}(r)$, $g_{\text{N-WFC}}(r)$, and $g_{\text{WFC-WFC}}(r)$ from $r=0$ to 1.5 Å. These can be seen in Fig. 3, where the dashed line is the C-WFC $g(r)$, the shaded area is the N-WFC $g(r)$, and the dotted line is the WFC-WFC $g(r)$ functions, respectively.

From the $g(r)$ analysis we calculated the carbon- sp^2 fraction for our networks and compared these to the results of using a coordination shell ($r=1.85$ Å) as shown in Table II. Table II reveals that while the sp^2 fraction using the WFC analysis is fairly consistent with the coordination sphere approach, the largest discrepancy occurred for the C_{62}N_2 -3.2 g/cm^3 network, where the sp^2 content using a coordination sphere was noticeably higher (16%) for the coordination sphere compared to using the WFC (3%). Inspection of the WFC's showed that several carbon ions, which were thought to be sp^2 , were actually bonded sp^3 with an elongated σ bond with a bond length greater than 1.85 Å. Other deviations from the coordination were due to either charged defects or an under-coordination of sites.

In the low-density networks C_{62}N_2 -2.45 and C_{56}N_8 -2.45 g/cm^3 , the carbon forms mostly C_3^0 sites with both networks containing a majority (nearly 80%) of three coordinate carbon atoms. The medium-density networks C_{62}N_2 -2.92 and C_{56}N_8 -2.95 g/cm^3 contain mostly C_4^0 sites, with the "increase" in nitrogen (from two to eight) leading

TABLE II. Details for the seven amorphous carbon nitride simulations. The percentile value is the coordination of carbon and nitrogen atoms in the simulated networks using a coordination sphere approach ($r = 1.85 \text{ \AA}$) and the value in brackets is calculated by analyzing the number of WFC's surrounding each atom.

Simulation (g/cm^3)	K (GPa)	Carbon coordination			Nitrogen coordination		
		2	3	4	2	3	4
C_{62}N_2 -2.45	274	1 (1)	76 (79)	23 (20)	50 (50)	50 (50)	
C_{56}N_8 -2.45	273	1 (1)	79 (79)	20 (20)	50 (50)	50 (50)	
C_{62}N_2 -2.95	306	0 (0)	39 (44)	61 (56)	50 (0)	50 (100)	
C_{56}N_8 -2.95	295	0 (2)	52 (48)	48 (50)	13 (13)	87 (74)	0 (13)
C_{62}N_2 -3.20	345	0 (0)	3 (16)	97 (84)		100 (100)	
C_{56}N_8 -3.20	336	1.6 (1)	23 (20)	76 (79)	50 (13)	50 (87)	
C_{60}N_4 -2.70	285	2	58	40	25	75	

to a reduction in the number of C_4^0 sites and an increase in C_3^+ and C_3^- defect sites. In the eight nitrogen network N_3^+ and N_4^+ defect sites are also present. The carbon atoms in these networks have a mix of three and four coordination, with the addition of nitrogen reducing the number of fourfold coordinated atoms.

The medium-density networks (C_{62}N_2 -2.95 and C_{56}N_8 -2.95 g/cm^3) can be compared to the density-functional tight-binding simulations of Köhler, Jungnickel, and Frauenheim and Weich, Widany, and Frauenheim³¹ who found similar average carbon and nitrogen coordination at similar N concentrations.

The WFC analysis shows most nitrogen atoms form a lone pair of electrons. Frauenheim *et al.*^{30,31} also found that nitrogen atoms tend to form lone pairs. However in our simulations we have found significantly fewer numbers of N_3^+ sites (sp^2 hybridized). Another feature of our simulations was that fourfold coordinated nitrogen sites were rare, with only one case of a N_4^+ in the 2.95 g/cm^3 eight nitrogen structure. This is in general agreement with Weich, Widany, and Frauenheim³¹ who found an average nitrogen coordination of 2.85 at 3.00 g/cm^3 indicating few if any N_4^+ at a similar density. A small number of N_4^+ sites is supported by the experimental results of Robertson and Davis³² who concluded that the low doping efficiency of N in *ta*-C was attributable to nitrogen forming nondoping N_3^0 sites.

The high-density networks C_{62}N_2 -3.2 and C_{56}N_8 -3.2 g/cm^3 show the largest differences in bonding two and eight nitrogen simulations. The carbon atoms are mostly four coordinated with the addition of more nitrogen dramatically decreasing the number of four coordinate carbon atoms and promoting the number of three coordinate carbon atoms.

The highest-density (3.2 g/cm^3) networks are dominated by sp^3 -carbon atoms, as shown in Tables II and III, with 97% in the two nitrogen and 76% in the eight nitrogen cases, respectively. As seen experimentally⁹ and computationally,³⁰ the increase in nitrogen has increased the carbon- sp^2 fraction.

Our results disagree with the theoretical study of Lu, He, and Ren³³ who studied carbon nitrides by minimizing the cohesive energy of 1000 atoms from random positions. They

found an increase in nitrogen was accompanied by an increase in the carbon- sp^3 / sp^2 fraction, whereas we have found an opposite effect. Lu, He, and Ren also found that an increase in nitrogen content was accompanied by a decrease in volume, whereas most experimental studies² have seen the opposite effect.

C. Ring statistics

The ring statistics of the networks were determined using a coordination sphere approach with a bond cutoff of 1.85 \AA . This approach was aided by checking whether the WFC lay between atoms in each ring, or even if some rings had been missed. The low-density structures show the majority of rings are five and seven membered.

Each of the networks reveal a different distribution of ring structures, as shown in Tables III and IV. Present in all simulations, are three- and four-membered rings, and in four instances these four-membered rings contain nitrogen atoms. A general trend is that the addition of nitrogen decreases the number of rings formed due to the formation of lone pairs, which is most noticeable at the highest density where threefold coordinated nitrogen atoms prevent the formation of many-ring structures compared to four coordinated C atoms.

The C_{56}N_8 -2.45 g/cm^3 network shown in Fig. 4 displays clear layering of the structure as suggested by Sjöström

TABLE III. All ring statistics. Bond-length cutoff used was 1.85 \AA ; the maximum ring size for the calculation was 12 atoms.

Simulation (g/cm^3)	Number of atoms in ring									
	3	4	5	6	7	8	9	10	11	12
C_{62}N_2 -2.45	1	1	10	3	8	3		5	2	
C_{56}N_8 -2.45		2	13	4	3	3	2			2
C_{62}N_2 -2.95	4	2	12	23	9	6	1	2		
C_{56}N_8 -2.95	2	5	8	14	10	11	3			2
C_{62}N_2 -3.20	2	2	21	29	26	8	1			
C_{56}N_8 -3.20	2	6	14	14	26	7	1			
C_{60}N_4 -2.70	3	3	8	12	7	4	3	1		

TABLE IV. N atom containing rings. The figure in brackets indicates the number of rings containing two nitrogen atoms in the ring. If the numbers are $X(Y)$, there are $X+Y$ rings containing nitrogen. There were no rings with more than two nitrogen atoms in a ring.

Simulation (g/cm^3)	Number of atoms in ring										
	3	4	5	6	7	8	9	10	11	12	
C_{62}N_2 -2.45			1		1				1		
C_{56}N_8 -2.45		1	4	3	2	(1)	2		1		(2)
C_{62}N_2 -2.95		1		3	2		2				
C_{56}N_8 -2.95		1	7	6	3		9	(1)	3		
C_{62}N_2 -3.20			2	5	4		3				
C_{56}N_8 -3.20		1	3	9	15	(1)	3	(1)	(1)		
C_{60}N_4 -2.70			1	3			1		1		

*et al.*²⁹ for a “fullerenelike” amorphous carbon nitride. In Table IV it is shown that in this network seven of the eight five-membered rings contain nitrogen, suggesting this is an energetically favorable configuration. This agrees with the Hartree-Fock-based calculations of Sjöström *et al.*,²⁹ which showed that curved sp^2 -carbon sheets with five-membered rings containing nitrogen were energetically favorable.

D. Comparison to neutron-diffraction data

To our best knowledge, there was no diffraction data available for the stoichiometries of the six simulated networks, so to compare our simulations with experiment, a seventh simulation was performed with 60 carbon and 4 nitrogen atoms with a density of $2.7 \text{ g}/\text{cm}^3$. The structure contained a majority (58%) of carbon atoms that were threefold coordinated. The radial distribution function $G(r)$ shown in Fig. 5(a) is compared to the experimental data from Walters *et al.*²¹ for a $2.7 \text{ g}/\text{cm}^3$ 5% nitrogen a -C:N; the agreement is good for both $G(r)$ and $S(Q)$ over the range at which comparison is valid. The region on $S(Q)$ at low Q ($< 2 \text{ \AA}^{-1}$) contains a contribution from the size and shape of the cell and should be ignored.

E. Bulk modulus

The calculated bulk modulus (K) was calculated by varying the lattice parameter by up to 1% and fitting elastic constants assuming a cubic system. The result for each network is shown in Table II. As expected, there is an increase in K with density. These calculations show that the addition of nitrogen on the order of 3%–11% does not significantly affect the bulk modulus of the amorphous structures. Our highest values are only 10% lower than those calculated by Lu, He, and Ren,³³ which is surprising considering the mass density used in their study was $6 \text{ g}/\text{cm}^3$, considerably higher than any of the networks simulated here.

F. Electronic density of states

The electronic density of states (EDOS) determined from the Kohn-Sham energy calculations are shown in Fig. 6. For

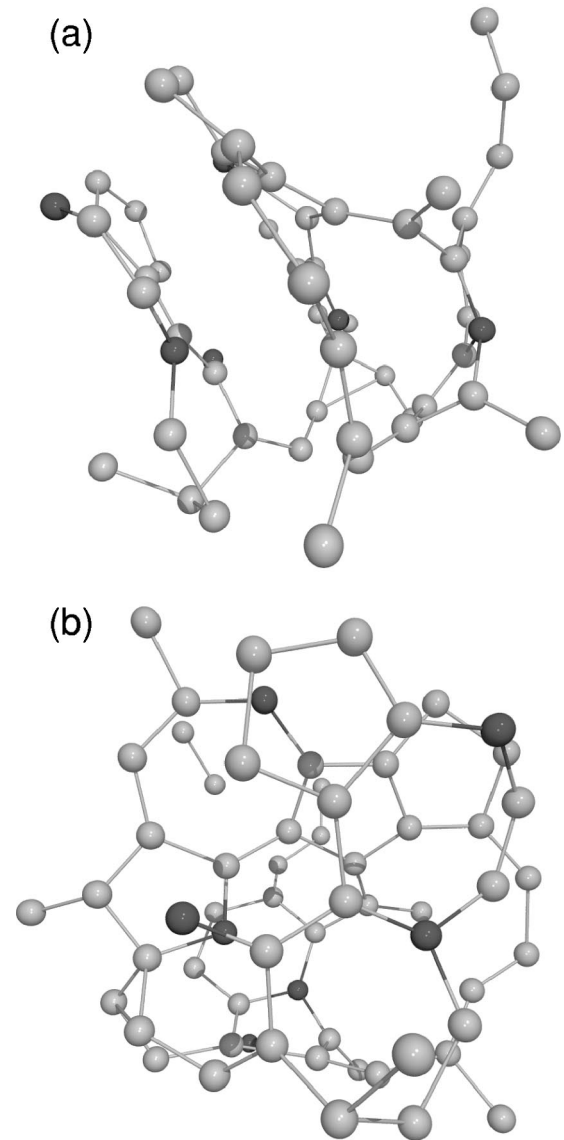


FIG. 4. Eight nitrogen $2.45\text{-g}/\text{cm}^3$ structures revealing fullerene-like layering, as suggested by Sjöström *et al.* (Ref. 29). (a) is a side view, while (b) is perpendicular to the first. Lighter atoms are carbon, darker atoms are nitrogen.

the sake of this comparison the Fermi energy is considered to be at the highest occupied state (solid lines). The unoccupied states are plotted with dashed lines. In general the higher densities have the fewest states in the “gap” while at lower densities there is no “gap” between the highest occupied molecular orbital and the lowest unoccupied molecular orbital (LUMO).

The two and eight nitrogen $2.45\text{-g}/\text{cm}^3$ EDOS, Figs. 6(e) and 6(f) have a large number of occupied and unoccupied states close to the Fermi energy, indicating these structures are potentially good conductors. Of interest is the intensity of the $1s$ - π^* region of the carbon K edge, which will be considered 0–5 eV above the LUMO. It is this feature that is used to obtain a measure of the π bonding in the material using electron energy-loss spectroscopy (EELS) or x-ray-absorption spectroscopy. There is a clear shoulder in the

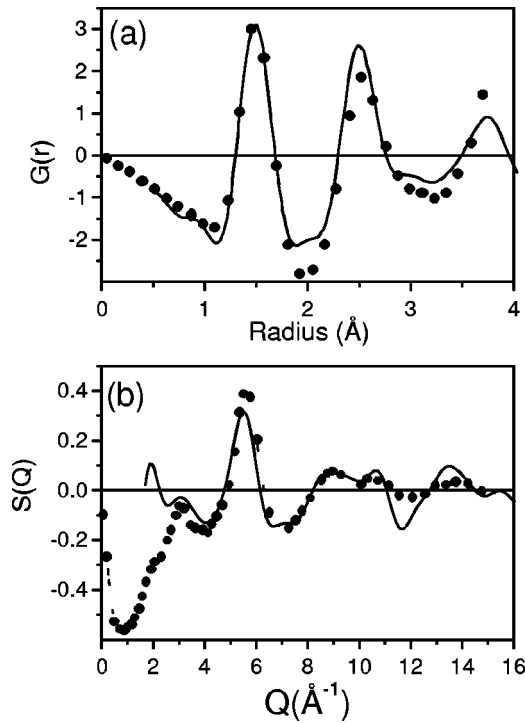


FIG. 5. The radial distribution function $G(r)$ and $S(Q)$ calculated for a 2.7-g/cm^3 C_{60}N_4 simulation. In (a) the solid line represents the simulated $G(r)$ smoothed using a bezier function, and the symbols represent scaled data from sample CN05 from Walters *et al.* (Ref. 21). In (b) the dotted line is the experimental data from the same sample CN05 from Walters *et al.* (Ref. 21).

$1s-\pi^*$ region in both the two and eight nitrogen cases at 2.45 g/cm^3 . A large $1s-\pi^*$ feature is a consequence of π bonding from the large number of threefold coordinated carbon atoms and the number of twofold coordinated carbon and nitrogen atoms in these structures. Table V compares the integral of the number of states in this region compared to the fraction of two- and threefold coordinated bonding in each of the networks. There is an increase in the number of states in this region as the number of nitrogen atoms increases (4.9 to 5.9). The enhancement of the $1s-\pi^*$ feature as N content increases (from 11% to 17%) has been seen experimentally by Hu, Yang, and Leiber,⁹ where it was coupled to a decrease in density favoring a more sp^2 -carbon network.

The intensity in the $1s-\pi^*$ diminishes as the density of the networks increase, and the edge of the occupied states becomes steeper. This effect was also seen by Köhler, Jungnickel, and Frauenheim.³⁰ The highest-density (3.2 g/cm^3) structure exhibits the largest “gap.” The low number of states between 0 and 5 eV is consistent with the characteristic “diamondlike” C and N K edges seen in experimental EELS spectra at low nitrogen concentrations.²

G. Calculations using the LSD approximation

In order to check whether the LDA was inhibiting certain bonding configurations and to explore the effect of removing electrons, calculations were performed on the simulated

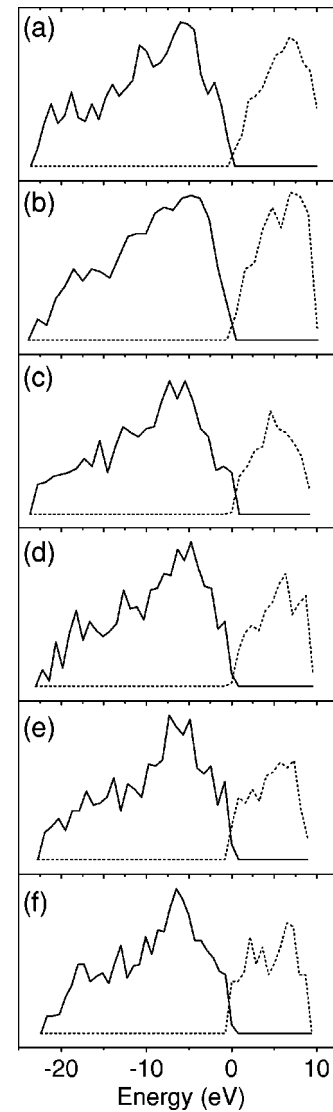


FIG. 6. The Kohn-Sham energies calculated for six simulations. (a)–(c) represent the 3.20- , 2.95- , and 2.45-g/cm^3 C_{62}N_2 , respectively, while (d)–(f) are for the 3.20- , 2.95- , and 2.45-g/cm^3 C_{56}N_8 , respectively. In the figure the solid line represents occupied states, the dotted line unoccupied states. Each plot is the sum of up to 10 configurations from the end of the 300-K anneal, each separated by approximately 0.01 ps.

TABLE V. Integrated unoccupied states grouped by number of nitrogen atoms per simulation.

Simulation (g/cm^3)	Unoccupied states	C sp^2+sp (%)
$\text{C}_{62}\text{N}_2\text{-}2.45$	4.9	80
$\text{C}_{56}\text{N}_8\text{-}2.45$	5.9	80
$\text{C}_{62}\text{N}_2\text{-}2.95$	3.6	44
$\text{C}_{56}\text{N}_8\text{-}2.95$	3.9	50
$\text{C}_{62}\text{N}_2\text{-}3.20$	3.2	16
$\text{C}_{56}\text{N}_8\text{-}3.20$	3.3	30

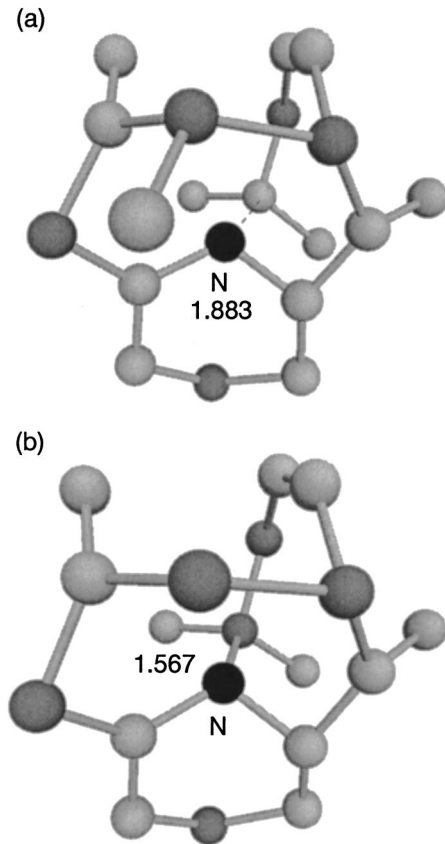


FIG. 7. Charging experiment for $C_{62}N_2$ 2.95 g/cm^3 showing (a) before an electron is removed from the structure and (b) a bond forming after. The distances shown are in Angstroms.

structures using LSD instead of LDA. A structure from near the end of the 300-K anneal for each density was chosen and a geometry optimization was performed using both LDA and LSD, and the structures were compared. There were no significant differences between the LDA and LSD optimized structures.

Further analysis of the LSD relaxed structures was then performed to study the effect of removing one electron. Charge removal corresponds to ionization and any subsequent structural relaxation would have important consequences in the study of $ta\text{-C:N}$ as an electronic material. In order to check the reversibility of any structural relaxation, the electron was replaced and the charge neutral structure was reoptimized. The effect of an electron removal was then determined by comparing the electronic charge densities and bond lengths of each structure at each of the steps.

The 2.45-g/cm^3 structures were not measurably affected by the removal of one electron. However in the 2.95-g/cm^3

two nitrogen network upon removal of an electron we observed a new bond between a threefold coordinated carbon atom and twofold coordinated nitrogen atom. This bond formation after charging is shown in Fig. 7. The formation of a bond is interesting because it showed that charging the system could result in structural change, and it also shows that this structural change may be localized on the nitrogen atoms for an N-doped $ta\text{-C}$ system.

In the eight nitrogen 3.20 g/cm^3 , one nitrogen atom switched bonds from one fourfold carbon to another threefold carbon as a result of charging. These observations support the concept that the nitrogen atoms are a source of local structural instability in agreement with experimental observations that high-density $ta\text{-C:N}$ is less stable in an electron beam than is undoped $ta\text{-C}$.² In addition, restoring the electron was found to only return the structure to its original condition provided that no new bonds had formed in the vicinity. This may explain the two-state conductivity that is observed in $a\text{-C:N}$.⁶ The local structural changes caused by the removal of an electron prevent the easy recapture of the electron to the nitrogen atom, giving rise to the observed hysteresis or “memory.”

IV. CONCLUSION

We have used *ab initio* molecular dynamics to study the structure and bonding of amorphous carbon nitride at a range of densities and nitrogen concentrations. By calculating the centers of maximally localized Wannier functions we are able to distinguish the different bonding types present in our networks. The main findings of this work are

1. The most common form of nitrogen bonding was found to be uncharged N_3^0 sites with a lone pair of electrons. Uncharged N_2^0 sites as well as charged N_4^+ , N_3^+ , and N_2^+ were also found.

2. The addition of nitrogen causes a decrease in the sp^3 fraction of carbon, and this effect is most severe at high densities. In addition to sp^3 - and sp^2 -bonded carbon, $sp(C_2^0)$, C_3^+ , and C_3^- defect sites were also observed.

3. Electronic density-of-states calculations show an increase in the $1s\text{-}\pi^*$ region at lower network densities and higher nitrogen concentrations as seen experimentally.

4. The removal of electrons from the networks caused structural changes, which could explain the two-state conductivity in $ta\text{-C:N}$ memory devices.

ACKNOWLEDGMENTS

The work was supported by a grant from the Australian Research Council. The authors would like to thank Nigel Marks and Brendan O'Malley for fruitful discussions.

*Electronic address: merchant@physics.usyd.edu.au

¹D. R. McKenzie, Rep. Prog. Phys. **59**, 1611 (1996).

²C. A. Davis, D. R. McKenzie, Y. Yin, E. Kravtchinskaya, G. A. J. Amaratunga, and V. S. Veerasamy, Philos. Mag. B **69**, 1133 (1994).

³B. Wei, B. Zhang, and K. E. Johnson, J. Appl. Phys. **83**, 2491

(1998).

⁴K. S. Yoo, B. Miller, R. Kalish, and X. Shi, Electrochem. Solid-State Lett. **2**, 233 (1999).

⁵V. S. Veerasamy, G. A. J. Amaratunga, C. A. Davis, A. E. Timbs, W. I. Milne, and D. R. McKenzie, J. Phys.: Condens. Matter **5**, L169 (1993).

- ⁶E. G. Gerstner and D. R. McKenzie, *Solid-State Electron.* **44**, 1641 (2000).
- ⁷A. Y. Liu and M. L. Cohen, *Science* **245**, 841 (1989).
- ⁸D. R. McKenzie, E. G. Gerstner, A. R. Merchant, D. G. McCulloch, P. E. Goa, N. C. Cooper, and C. M. Goringe, *Int. J. Mod. Phys. B* **14**, 230 (2000).
- ⁹J. Hu, P. Yang, and C. M. Leiber, *Phys. Rev. B* **57**, R3185 (1998).
- ¹⁰N. A. Marks, D. G. McCulloch, and D. R. McKenzie, *Phys. Rev. B* (to be published).
- ¹¹P. L. Silvestrelli, N. Marzari, D. Vanderbilt, and M. Parrinello, *Solid State Commun.* **107**, 7 (1998).
- ¹²J. Hütter, A. Alvi, T. Deutschand, M. Bernasconi, St. Goedecker, D. Marx, M. Tuckerman, and M. Parrinello, computer code CPMD (Max Planck Institute für Festkörperforschung, Stuttgart, Germany, and IBM Zurich Research Laboratory, Zurich, Switzerland, 1995–1999).
- ¹³N. A. Marks, D. R. McKenzie, B. A. Pailthorpe, M. Bernasconi, and M. Parrinello, *Phys. Rev. B* **54**, 9703 (1997).
- ¹⁴D. G. McCulloch, D. R. McKenzie, and C. M. Goringe, *Phys. Rev. B* **61**, 2349 (2000).
- ¹⁵G. Galli, R. M. Martin, R. Car, and M. Parrinello, *Phys. Rev. B* **42**, 7470 (1990).
- ¹⁶D. G. McCulloch, D. R. McKenzie, and C. M. Goringe, *J. Appl. Phys.* **88**, 5028 (2000).
- ¹⁷P. Stumm, D. A. Drabold, and P. A. Fedders, *J. Appl. Phys.* **81**, 1289 (1997).
- ¹⁸N. Troullier and J. L. Martins, *Phys. Rev. B* **43**, 1993 (1991).
- ¹⁹A. D. Becke, *Phys. Rev. A* **38**, 3098 (1988).
- ²⁰C. Lee, W. Yang, and R. G. Parr, *Phys. Rev. B* **37**, 785 (1988).
- ²¹J. K. Walters, M. Kühn, C. Spaeth, H. Fischer, F. Fichter, and R. J. Newport, *Phys. Rev. B* **56**, 14 315 (1997).
- ²²F. Demichelis, X. F. Fong, S. Schreite, A. Tagliaferro, and C. E. Martino, *Diamond Relat. Mater.* **4**, 361 (1995).
- ²³N. A. Marks, *Phys. Rev. B* **56**, 2441 (1997).
- ²⁴N. Marzari and D. Vanderbilt, *Phys. Rev. B* **56**, 12 847 (1997).
- ²⁵G. Berghold, C. J. Mundy, A. H. Romero, J. Hutter, and M. Parrinello, *Phys. Rev. B* **61**, 10 040 (2000).
- ²⁶B. E. Warren, *X-Ray Diffraction* (Addison-Wesley, Reading, MA, 1969).
- ²⁷S. R. Elliot, *Physics of Amorphous Materials* (Longman Scientific and Technical, Essex, 1984).
- ²⁸D. S. Franzblau, *Phys. Rev. B* **44**, 4925 (1991).
- ²⁹H. Sjöström, S. Stafström, M. Boman, and J.-E. Sundgren, *Phys. Rev. Lett.* **75**, 1336 (1995).
- ³⁰Th. Köhler, G. Jungnickel, and Th. Frauenheim, *Phys. Rev. B* **60**, 10 864 (1999).
- ³¹F. Weich, J. Widany, and Th. Frauenheim, *Phys. Rev. Lett.* **78**, 3326 (1997).
- ³²J. Robertson and C. A. Davis, *Diamond Relat. Mater.* **4**, 441 (1995).
- ³³Y. F. Lu, Z. F. He, and Z. M. Ren, *J. Appl. Phys.* **86**, 5417 (1999).